Establishment in Severe Combined Immunodeficiency Mice of Subrenal Capsule Xenografts and Transplantable Tumor Lines from a Variety of Primary Human Lung Cancers: Potential Models for Studying Tumor Progression – Related Changes

Jean-Claude Cutz,[1,5] Jun Guan,[1] Jane Bayani,[5] Maisa Yoshimoto,[5] Hui Xue,[1] Margaret Sutcliffe,[1] John English,[3] Julia Flint,[3] Jean LeRiche,[2] John Yee,[4] Jeremy A. Squire,[5,6] Peter W. Gout,[1] Stephen Lam,[2] and Yu-Zhuo Wang[1]

Abstract

Purpose: Lung cancer is a biologically diverse disease and relevant models reflecting its diversity would facilitate the improvement of existing therapies. With a view to establishing such models, we developed and evaluated xenografts of a variety of human lung cancers.

Experimental Design: Using nonobese diabetic/severe combined immunodeficiency mice, subrenal capsule xenografts were generated from primary lung cancer tissue, including moderately and poorly differentiated squamous cell carcinoma, adenocarcinoma, adenosquamous carcinoma, small cell carcinoma, large cell undifferentiated carcinoma, and carcinosarcoma. After 4 to 12 weeks, xenografts were harvested for serial transplantation and comparison with the original tissue via histologic, chromosomal, and cytogenetic analyses.

Results: Xenografts were successfully established. H&E staining showed that xenografts retained major histologic features of the original cancers. Immunohistochemistry and fluorescence *in situ* hybridization confirmed the human origin of the tumor cells and development in xenografts of murine supportive stroma. Four transplantable lines were developed from rapidly growing tumors (>5 generations), i.e., a small cell lung carcinoma, large cell undifferentiated carcinoma, pulmonary carcinosarcoma, and squamous cell carcinoma. Analyses including spectral karyotyping, comparative genomic hybridization, and fluorescence *in situ* hybridization, revealed that the xenografts were genetically similar to the original tumors, showing chromosomal abnormalities consistent with karyotypic changes reported for lung cancer.

Conclusions: The subrenal capsule xenograft approach essentially provides a living tumor bank derived from patient material and a means for isolating and expanding specific cell populations. The transplantable tumor lines seem to provide good models for studying various aspects of tumor progression and a platform for developing novel therapeutic regimens, with the possibility of patient-tailored therapies.

Authors' Affiliations: Departments of [1]Cancer Endocrinology and [2]Cancer Imaging, BC Cancer Agency, Departments of [3]Pathology and [4]Surgery, Vancouver General Hospital, Vancouver, British Columbia, [5]Department of Applied Molecular Oncology, Ontario Cancer Institute, University Health Network, and [6]Departments of Laboratory Medicine and Pathobiology, and Medical Biophysics, University of Toronto, Toronto, Ontario, Canada

Received 2/2/06; revised 4/25/06; accepted 5/1/06.

Grant support: National Cancer Institute of Canada, the British Columbia Lung Association (Y.Z. Wang) and Genome Canada (S. Lam). J-C. Cutz is supported by the Canadian Institutes of Health Research Strategic Training Program Grant STP-53912.

The costs of publication of this article were defrayed in part by the payment of page charges. This article must therefore be hereby marked *advertisement* in accordance with 18 U.S.C. Section 1734 solely to indicate this fact.

Note: J-C. Cutz, J. Guan, and J. Bayani contributed equally to this study.

Requests for reprints: Yu-Zhuo Wang, Department of Cancer Endocrinology, BC Cancer Agency, Research Centre, 675 West 10th Avenue, Vancouver, British Columbia, Canada V5Z 1L3. Phone: 604-675-8013; Fax: 604-675-8183; E-mail: ywang@bccrc.ca.

doi:10.1158/1078-0432.CCR-06-0252

Lung cancer is a biologically diverse disease. Clinically and pathologically, there is a major distinction between small cell lung cancer (SCLC) and non–small cell lung cancer (NSCLC), with the latter including large cell carcinoma, squamous cell carcinoma (SQCC), and adenocarcinoma (1). It is therefore unlikely that one treatment modality will be effective against all forms of this disease. Accordingly, there is a need for clinically relevant models for lung cancer that reflect the diversity of the disease.

The most commonly used lung cancer models consist of xenografts generated by injecting cultured human cancer cells s.c. into immunodeficient mice (2). Typically, the cancer cells used are derived from advanced, highly aggressive, or poorly differentiated neoplasms (3, 4). Furthermore, the developing tumors lack their original microenvironment, including tumor-associated stroma, which has recently been shown to be important in tumor development and progression (5). Such cancer cell line xenograft models in general show limited ability

in predicting clinical efficacy of anticancer agents (6). To address these limitations, efforts have been made to grow histologically intact human lung tumor tissue in a variety of graft sites in immunodeficient mice. Engraftment, however, was only successful when highly advanced cancers were used and tumor take rate was in general exceedingly low (7).

Of the various graft sites available, the subrenal capsular (SRC) site offers the particular advantage of very high organ perfusion and potentially rapid development of graft microvasculature (8). In spite of this, SRC grafting of human tumor tissue has been plagued by poor tumor take rates for a number of decades. Recently, however, we have been able to successfully apply this technique for grafting a variety of primary human tumor tissues in severe combined immunodeficiency mice. Using tissue specimens from cancers of the prostate, breast, colon, kidney, and lymph nodes, we have been able to consistently achieve engraftment rates of >95% (7, 9, 10).

In the present study, we used the SRC grafting technique to establish a variety of human lung cancer tissue xenografts in severe combined immunodeficiency mice with a high take rate and retention of major histologic features. Furthermore, xenografts were obtained showing various levels of tumor cell differentiation, including well and moderately differentiated types. In four cases, transplantable lung tumor lines were established. A variety of analyses, including spectral karyotyping (SKY), comparative genomic hybridization (CGH), and interphase fluorescence *in situ* hybridization (FISH) were used to (*a*) confirm the presence of engrafted human tissue within the mouse kidney capsule, (*b*) identify chromosomal changes in early generation xenografts and compare them to later generations, and (*c*) determine whether the resulting xenograft lines were similar to the original tumor before engraftment. These findings suggest that the SRC methodology provides a superior means for establishing xenograft tumors. The high success rate of engraftment holds the potential for studying disease progression and evaluating potential therapies that can be more individually tailored.

Materials and Methods

Materials and animals. Chemicals, stains, solvents, and solutions were obtained from Sigma-Aldrich Canada, Ltd. (Oakville, Ontario, Canada), unless otherwise indicated. Six- to eight-week-old severe combined immunodeficiency/nonobese diabetic mice were bred by the BC Cancer Research Centre Animal Resource Centre, BC Cancer Agency (Vancouver, British Columbia, Canada).

Procurement of lung cancer tissue. Lung tissue specimens were obtained at the Vancouver General Hospital and BC Cancer Agency from 14 patients with written consent and approval by the UBC/BCCA Research Ethics Committee. Pneumonectomy, lobectomy, or wedge resections done at the Vancouver General Hospital were processed within 30 minutes at Vancouver General Hospital Department of Pathology. Tumor tissue in the lung specimens was exposed by sharp dissection and serially sectioned using a sterile scalpel blade. Slivers of tissue from grossly abnormal and/or normal areas were sampled and immediately placed in ice-cold HBSS. The bulk of the lung specimen was then fixed in formalin for routine pathologic assessment. Bronchial biopsy tissue was obtained from the Vancouver Cancer Centre, BC Cancer Agency using endoscopic technique and processed as above. The age and sex of the patients, any prior treatment, and histopathology of their tumors are presented in Table 1. The mean age was 63 years (range, 49-73 years) with nine males and five females.

SRC grafting and harvesting of tissues. The establishment of grafted tissues was carried out as follows and according to methods previously published by this group (10, 11). Briefly, tissue fragments selected for grafting (pregraft tissues) were stored at 4°C in HBSS supplemented with antibiotics. Within two hours, each sample was cut into multiple $3 \times 3 \times 1$ mm pieces (2-12 pieces/specimen) to be grafted under the renal capsules of two to six severe combined immunodeficiency/nonobese diabetic mice (one to two grafts/kidney). When possible, a portion was fixed for histologic analysis. A skin incision of ~2.0 cm was made along the dorsal midline of an anesthetized mouse. With the animal lying on its side, an incision was then made in the body wall slightly shorter than the long axis of the kidney. The kidney was slipped out of the body cavity by applying pressure on the other side of the organ using a forefinger and thumb. The exteriorized kidney was rested on the body wall and a no. 5 fine forceps were used to gently pinch and lift the capsule from the renal parenchyma to allow a 2 to 4 mm incision in the capsule using fine spring-loaded scissors. A pocket between the kidney and the parenchyma was then created by blunt dissection. Care was taken not to damage the renal parenchyma and thus prevent bleeding. The graft was transferred to the surface of the kidney using blunt-ended forceps. The cut edge of the renal capsule was lifted with a pair of fine forceps and the graft inserted into the pocket under the capsule using a polished glass pipette. Two or three grafts per kidney could be placed under the renal capsule. The kidney was then gently eased back into the body cavity and all body wall and skin incisions were sutured. Mice were housed in same-sex groups of three in microisolators with free access to food and water and their health was monitored daily. Animal care and experiments were carried out in accordance with the guidelines of the Canadian Council on Animal Care.

First-generation implant growth was assessed by palpation and harvested at 30 days or up to 60 days postgrafting. At harvesting, mice were sacrificed in a CO_2 chamber and grafts were collected for histologic evaluation, regrafting, or snap-freezing in liquid nitrogen. Rapidly growing tumors were maintained by serial transplantation for growing periods as short as 20 days; only one kidney per animal was used in the case of locally invasive tumors. For slow-growing grafts, collection or regrafting was done after a maximal growth period of 2 months. In some cases, liver, lung, spleen, brain, and lymphoid tissue were examined grossly and histologically for metastases.

Histopathology and immunohistochemistry. The original pathologic specimens and their transplants were fixed in 10% neutral buffered formalin, and processed to paraffin. Sections were cut on a microtome and mounted on glass slides. Sections were dewaxed in Histoclear (National Diagnostic, Atlanta, GA) and hydrated in graded alcoholic solutions and distilled water. For histopathology, routine H&E staining was carried out. For immunohistochemistry, endogenous peroxidase activity was quenched with 0.5% hydrogen peroxide in methanol for 30 minutes followed by washing in PBS (pH 7.4) and nonspecific binding blocked using 5% normal goat or donkey serum in PBS (as appropriate) for 30 minutes. Sections were then incubated with the primary antibodies [anti-Ki-67 (Immunotech, Westbrook, ME) and antihuman mitochondrial antibody (Chemicon, Temecula, CA)], overnight at 4°C or with nonimmune mouse IgG (Zymed Corp., South San Francisco, CA) at the same concentration as the primary antibodies (used as negative controls). Sections were then washed with PBS and incubated with the appropriate biotinylated secondary antimouse immunoglobulin (Amersham International, Arlington Heights, IL), diluted with PBS at 1:200, for 30 minutes at room temperature. Sections were then washed in PBS (three 10-minute washes), and incubated with avidin-biotin complex (Vector Laboratories, Foster City, CA) for 30 minutes at room temperature. Following a further 30 minutes of washing in PBS, immunoreactivity was visualized using 3′,3′-diaminobenzidine in PBS and 0.03% H_2O_2. Sections were counterstained with hematoxylin, and dehydrated in graded alcohols.

Primary tissue culture and metaphase preparation for karyotypic analysis. Tumor xenograft fragments were finely minced and, if

Table 1. Clinical and pathologic features of patient material used for xenografting

Patient no.	Age/sex	Pathologic diagnosis	Stage	Prior treatment	Follow-up status	Follow-up period after surgery or biopsy
1	64/male	Squamous metaplasia	N/A	Previous lung resection for SQCC	Lost in follow-up	0
2	52/male	PD-SQCC	$T_2N_0M_0$	No	Lost in follow-up	0
3	68/male	SCLC	Extensive	CE with radiation; recurrence treated with VDE	Brain metastases, died	10 days
4	64/male	PD-SQCC	$T_1N_0M_0$	No	Additional wedge resection for SQCC	4 months, alive
5	49/male	Carcinoid	N/A	No	Tumor enlargement; tracheal metastases, small cell carcinoma	30 months, alive
6	64/female	PD-SQCC	$T_2N_1M_1$	No	Brain metastases, died	8 months
7	56/female	MD-SQCC	$T_1N_0M_0$	No	Lost in follow-up	0
8	66/female	SCLC	Extensive	CE with radiation	Liver metastases, died	13 months
9	69/male	Carcinosarcoma	$T_2N_0M_0$	No	Lost in follow-up	0
10	73/female	MD-AC	$T_2N_2M_0$	No	Resection of vertebral metastasis	29 months, alive
11	68/female	WD-AC	$T_3N_1M_0$	No	No known metastasis or recurrence	20 months, alive
12	52/male	PD-SQCC	$T4N_3M_1$	No	Brain metastases, died	6 months
13	67/male	PD-SQCC	$T_2N_1M_0$	No	No known metastases or recurrence	27 months, alive
14	64/male	SCLC	Limited	CE	Pulmonary recurrence	28 months, alive

NOTE: Patient age, sex, pathologic diagnosis, and stage at time of surgery or biopsy (if applicable) are indicated. Treatment prior to biopsy is indicated in patients with SCLC. Any significant events postsurgery/biopsy are noted when available.
Abbreviations: CE, cisplatin-etoposide; VDE, vincristine-doxorubicin-etoposide.

required, collagenase-treated overnight and cultured in α-MEM or RPMI 1640 containing fetal bovine serum (20%; Sigma, Toronto, Ontario, Canada), L-glutamine (1%), and penicillin-streptomycin (1%; Life Technologies, Toronto, Ontario, Canada). Cultures were harvested within 5 days by treatment with 0.1 μg/mL Colcemid (Life Technologies) for 2 to 3 hours, followed by osmotic swelling in KCl solution (0.075 mol/L), and fixed in methanol/acetic acid (3:1). Metaphase spreads were obtained by drop-wise application and drying of the fixed cell suspensions onto glass microscope slides under high humidity. Normal human lymphocytes were Ficoll-Hypaque–separated (12), harvested, and fixed as described above.

SKY analysis. Slide pretreatment, hybridization, posthybridization washes, detection, and SKY were done on tumor metaphase cells according to the manufacturer's instructions (Applied Spectral Imaging, Ltd., Carlsbad, CA) and as previously reported (13, 14). Spectral images were acquired and analyzed with an SD200 Spectral Bio-Imaging System and SKYVIEW software version 1.2 (Applied Spectral Imaging, Ltd., Migdal Ha'Emek, Israel) attached to a Zeiss Axioplan-2 microscope (Carl Zeiss Canada, Ltd., Toronto, Ontario, Canada). 4′,6-Diamidino-2-phenylindole (DAPI) banding was used in conjunction with SKY to identify chromosomal bands involved in rearrangements. The karyotypes described indicate clonal aberrations, specifically when a numerical gain was seen in at least two cells, a chromosomal loss seen in at least three cells, and a chromosomal rearrangement in at least two cells, as recommended by the 1995 International Standards for Human Cytogenetic Nomenclature (15). When sufficient metaphase cells of adequate quality were present, 10 metaphase cells were analyzed.

Paraffin FISH. To confirm that resulting tumors were of human origin, two-color FISH was done using directly labeled mouse and human species-specific, pan-centromeric Star*FISH DNA probes (Cedarlane Laboratories, Hornby, Ontario, Canada). Formalin-fixed sections (10 μm) were placed in 2× SSC at 75°C for 20 minutes and then digested in 0.25 mg/mL of proteinase K/0.1× SSC for 20 minutes at 45°C. Following a dehydration series of ethanols, co-denaturation of the tissue and probe was done at 80°C for 10 minutes followed by a 16-hour hybridization in a HYBrite slide incubator (Abbott Laboratories, Abbott Park, IL) at 37°C. Posthybridization washes were carried out according to the manufacturer's instructions. Paraffin FISH using the Vysis locus-specific probe for MYCC and centromere 8 (Abbott Laboratories) was also used to confirm the amplification of MYCC in tissues as well as the use of the Vysis Urovision (Abbott Laboratories) panel of probes for centromeres 3 (Spectrum Red), 7 (Spectrum Green), 17 (Aqua), and the gene-specific probe for 9p21 (Spectrum Gold) to confirm ploidy.

Single cell CGH. To ensure reliable CGH profiling, all pregraft and postgraft tissues were first examined by pathologists (J-C. Cutz and M. Sutcliffe) using H&E-stained sections, immunohistochemistry, and/or FISH to determine the extent of contaminating lymphocytic infiltration. Only tissues with minimal (<30%) contamination, by infiltrating lymphocytes of human or mouse origin, were selected for CGH profiling. In addition, only samples providing at least 150 ng of genomic DNA were used to minimize sampling bias from a small subset of tumor cells. Based on these criteria, the following tissues were selected: LU6-SCLC postgraft, both early and later generation; LU7-LCUC (large cell undifferentiated carcinoma), both pregraft and

postgraft, early generation, and LU13-CaS (carcinosarcoma), pregraft tumor. Groups of tumor cells were isolated from dewaxed paraffin sections stained with Histogene stain (Arcturus BioScience, Inc., Mountain View, CA) by direct microdissection under a dissecting microscope and placed in 15 to 30 μL proteinase K digestion buffer overnight at 56°C provided by a DNA extraction kit (Qiagen DNA Micro Kit, Mississauga, Ontario, Canada). The DNA was extracted according to the manufacturer's instructions, quantified by standard spectrophotometric methods and assessed by gel electrophoresis. DNA (150 ng) was amplified as described by Klein et al. (16) and the CGH assay was carried out as described by Stoecklein et al. (17). The labeled tumor and normal DNA was hybridized to metaphase spreads, imaged and analyzed using the Vysis Quips Imaging System (Vysis, Inc. Downers Grove, IL).

Results

Establishment of xenografts from lung tissue. SRC grafting of lung tissue samples resulted in all cases in viable grafts as revealed by gross and histologic examination (Table 2; Figs. 1–3). Figure 1 illustrates the histologic features of pregraft tissues and early generation xenografts from representative tissues of SQCC, adenocarcinoma, and SCLC. Five benign tissue grafts from three patients were sustained without appreciable growth. One graft of carcinoid tumor (LU9) and one from SCLC (LU12) yielded fibrous stroma only. Although most of the cancer xenografts exhibited volume doubling times well beyond 2 months, some lines showed much shorter doubling times: LU6-SCLC (4 days), LU7-LCC (20 days), LU13-CaS (25 days), and LU16-SQCC (10 days). These lines were used for the development of transplantable tumors in view of their relatively rapid growth. From a total of 168 first-generation tissue implantations, the net engraftment rate was >95%. Subsequent generations of tumor tissue grafts showed even higher take rates.

Histologic appearance of xenografts and comparison with pregraft tissues. Pregraft and postgraft histology for each case was compared (Table 2). In addition, pregraft tissues were compared with available diagnostic surgical material to further assess sampling representation of the original tumor.

- Normal lung tissues. Grafted bronchial mucosa exhibited normal histologic features such as ciliated respiratory epithelium (Fig. 2A). Grafted lung parenchyma showed dramatic expansion of the interstitium by connective tissue. The alveolar spaces assumed a simple tubular morphology lined by prominent alveolar cells (data not shown).
- SQCC. The four cases of SQCC consisted of one moderately differentiated keratinizing and three poorly differentiated squamous carcinomas. Typical squamoid features were observed, including intercellular bridges, dyskeratotic cells, and keratin pearl formation in some instances.
- Adenocarcinoma. The case of well differentiated and of a moderately differentiated adenocarcinoma showed typical glandular formations of tumor cells with prominent nucleoli.
- Adenosquamous carcinoma. The sole case of an adenosquamous carcinoma featured squamoid cells forming abortive glands and cystic spaces (Fig. 2B and C).
- Large cell undifferentiated carcinoma. Pre-engraftment and early generation tumors are illustrated in Fig. 2D and E for LU7-LCUC. Electron microscopy revealed intracytoplasmic dense-core or neurosecretory granules indicating neuroendocrine features (Fig. 2F). However, the tumor cells were negative for synaptophysin and chromogranin A (data not shown). Local tissue invasion and metastases to liver, lung, and lymph node were observed grossly and confirmed by immunohistochemistry (Fig. 2G and H) and FISH (Fig. 2I).

Table 2. Comparison of tissue histology pregrafting and postgrafting

Patient no.	Xenograft line	Pregraft tissue morphology	Postgraft morphology
1	LU1	Immature squamous metaplasia	Ciliated bronchial epithelium
	LU2		
2	LU3-ADSQ	Mixed SQCC-ADSQ	ADSQ
	LU4	Benign peribronchial tissue	Benign peribronchial tissue
	LU5	Benign lung parenchyma	Benign lung parenchyma
3	LU6-SCLC	SCLC	SCLC
4	LU7-LCC	PD-SQCC and LCUC	LCUC
	LU8	Benign lung parenchyma	Benign lung parenchyma
5	LU9	Carcinoid	Stromal tissue
6	LU10-SQCC	PD-SQCC	PD-SQCC
7	LU11-SQCC	MD-SQCC	MD-SQCC
8	LU12	SCLC	Stromal tissue
9	LU13-CaS	Carcinosarcoma	Sarcoma
10	LU14-AC	MD-AC	MD-AC
11	LU15-AC	WD-AC	WD-AC
12	LU16-SQCC	PD-SQCC	PD-SQCC
13	LU17-SQCC	PD-SQCC	PD-SQCC
14	LU18-SCLC	SCLC	SCLC

NOTE: Patient numbers correspond to those in Table 1. Lung ("LU") tissue xenografts were numbered consecutively. Tumor xenografts were given an additional designation according to their postgraft histology.
Abbreviations: ADSQ, adenosquamous carcinoma; PD, poorly differentiated; MD, moderately differentiated; WD, well-differentiated.

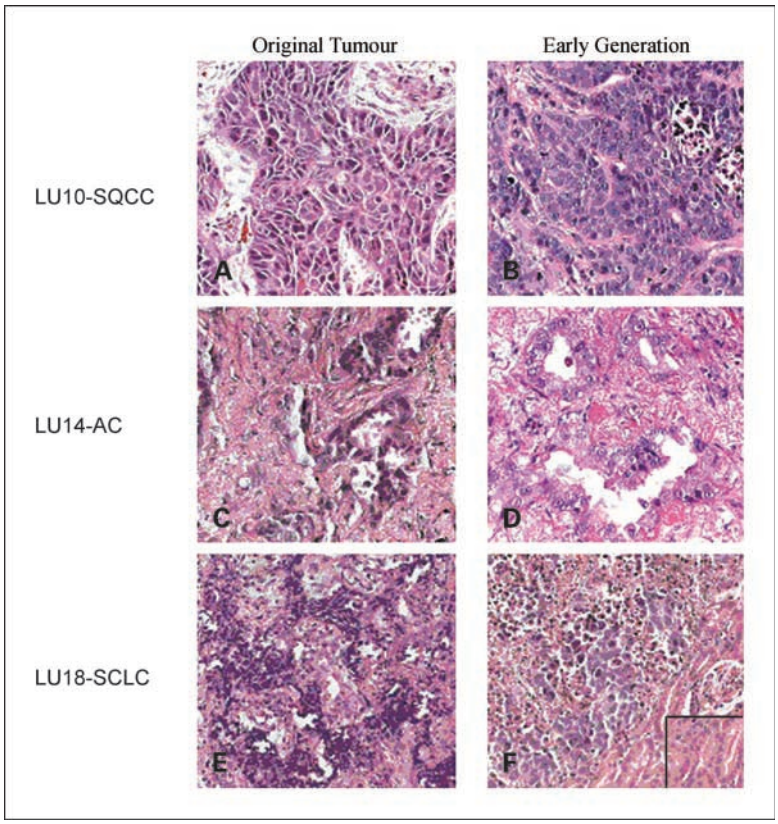

Fig. 1. Representative H&E stained tissue of pregraft tumor tissue (*left*) and corresponding early-generation xenografts (*right*) for cases of poorly differentiated SQCC (*LU10-SQCC, A* and *B*); moderately differentiated adenocarcinoma (*LU14-AC, C* and *D*), and small cell carcinoma (*LU18-SCLC, E* and *F*). Inset, an area of adjacent host mouse kidney (*F*).

The tumor cells grew in solid sheets with a monotonous appearance and moderate, pale cytoplasm.

- SCLC. All transplants from the three cases of SCLC exhibited typical histologic features such as spindle cell morphology with minimal cytoplasm and nuclear molding with hyperchromatic nuclei. Tumor cells were arranged in sheets and ribbons of variable cellularity often surrounded by areas of necrosis and/or hemorrhage.
- Carcinosarcoma. LU13-CaS was derived from a rare mixed mesenchymal-epithelial tumor, comprised of sarcomatous cells with areas of osteoid and chondroid formation. The epithelial component consisted primarily of LCUC (Fig. 2J and K). Transplanted tumors exhibited highly aggressive cytologic features such as marked nuclear pleomorphism or anaplasia with multilobed nuclei or multinucleation. Smudged chromatin and bizarre mitotic figures were frequent. The grafts showed a sarcomatoid morphology without areas of definitive mature mesenchymal or epithelial differentiation. FISH using both mouse pan-centromeric and human pan-centromeric probes (Fig. 2L) revealed the presence of infiltrating mouse stroma into the engrafted human tissue.

Taken together, the data indicate that during the first 2 months of transplantation, both slow- and fast-growing primary lung cancer tissue xenografts were histologically very similar to the original tumors, and hence, phenotypically quite stable.

Establishment of transplantable tumor lines and histopathologic analysis. The four fast-growing tumor xenograft lines selected for serial transplantation, LU6-SCLC, LU7-LCUC, LU13-CaS, and LU16-SQCC all produced several generations (more than five) of tumor tissue with no apparent alteration in cytology or architecture (Fig. 3). Cell viability was high as assessed by H&E staining and Ki-67 immunolabeling. The human origin of these transplantable tumor lines was confirmed by use of both human-specific anti-Ki-67 and anti-mitochondrial antibodies, as well as species-specific FISH probes for pan-centromeric sequences (Fig. 2I and L).

Correlation between xenograft behavior and patient clinical outcome. Of the 12 patients with a diagnosis of malignancy and representative xenograft tissue, six showed no evidence of metastases (nodal or distant) at the time of surgery, and none of the corresponding xenografts went on to metastasize within 60 days of engraftment. Tumor tissue obtained from five patients with evidence of metastatic disease did not produce metastases in the mice. However, in the case of LU7-LCUC, in which the original tumor was not clinically associated with metastases, xenografts from all generations exhibited local tissue invasion and distant metastases in the mice.

Cytogenetic analysis of transplantable tumor lines. Metataphase spreads were obtained from xenograft primary cultures. SKY analysis was done on the four transplantable tumor lines (LU6-SCLC, LU7-LCUC, LU13-CaS, and LU16-SQCC) and is summarized in Table 3 and illustrated in Fig. 4 (for LU6-SCLC) and Fig. 5 (for LU7-LCUC, LU13-CaS, and LU16-SQCC). The overall mitotic indices of the tumors were varied, thus limiting the number of metaphases available for SKY analysis. In some cases, poor chromosome morphology prevented complete karyotypic descriptions.

LU6-SCLC was found to be hypodiploid with both complex and simple clonal chromosomal aberrations (Fig. 4A-C). The

most conspicuous aberrations were the large chromosomes composed of material from chromosome 8. SKY analysis identified these aberrations as translocations involving chromosomes 8 and Y (Fig. 4B and C) and chromosomes 8 and 22 (Fig. 4B and C). Moreover, the relative size of the chromosome 8 material and banding pattern reflected the likelihood of gain or amplification of chromosome 8q. SKY analysis of an early xenograft and later generation xenograft revealed the same karyotypic changes, implying a faithful maintenance of this karyotype across several xenograft generations. LU7-LCUC showed a mainly diploid and clonal karyotype with less complex structural changes than LU6-SCLC (Fig. 5A). LU13-CaS possessed a highly complex, near-tetraploid karyotype with numerous complex structural rearrangements, dicentric and ring chromosomes as well as evidence of triradial formation (Fig. 5C, inset). Poor chromosome morphology of the cytogenetic preparation precluded a complete karyotypic description; however, identification of some of the clonal chromosomal aberrations was possible for some cells and are tabulated in Table 3. The SQCC tumor, LU16-SQCC, also showed a karyotype that was complex and in the triploid range (Fig. 5G; Table 3). Like LU13-CaS, chromosomal aberrations involving more than three chromosomes were common, as well as the presence of dicentric chromosomes. In addition, very few normal chromosomes were identified (Table 3; Fig. 5G).

To better characterize the genomic profile of these xenografts, CGH was done (Table 3). Xenografted tumor cells were microdissected from paraffin-embedded sections and DNA was extracted, amplified, and labeled for CGH. In some cases, however, the condition of the original paraffin block and tissue resulted in degraded DNA not suitable for amplification. For LU6-SCLC, CGH was done on both the early and late xenografts. The early xenograft CGH profile confirmed the amplification of 8q, identified by SKY as high-level amplification of the regions of 8q13 and 8q23 (Fig. 4D), likely produced by the large chromosomal rearrangement between Y and 8, as well as the structure involving chromosomes 8 and 22. FISH analysis using the MYCC probe (8q24) confirmed the amplification of the 8q23/24 region (Fig. 4E) and showed a pattern of signal hybridization consistent with the chromosomal structures identified by SKY. The detected gain of 11p11-p12 in the early graft corresponds to the complex structural rearrangement involving chromosome 20 and the gain of 5q14-q23 corresponds to the described i(5q) by SKY. The later generation profile showed similar changes, including the retention of the 8q amplifications and loss of 8p. For LU7-LCUC, no viable tumor tissue before grafting was available for cytogenetic analysis; only CGH and FISH could be done (Table 3). The CGH profile of the early graft revealed similar findings as the tumor before engraftment, including the loss of 1p36-pter and 12q24-qter, and gain of 5 and 8q. The CGH profiles of the early and late xenograft were found to be in concordance with the chromosomal changes detected by SKY, including the loss of 1p material likely due to the unbalanced translocations involving chromosome 1. Moreover, FISH analysis using a cocktail probe set consisting of centromeres 3, 7, and 17, and a locus-specific probe for 9p21, confirmed the diploid status of the original tumor, thus indicating the

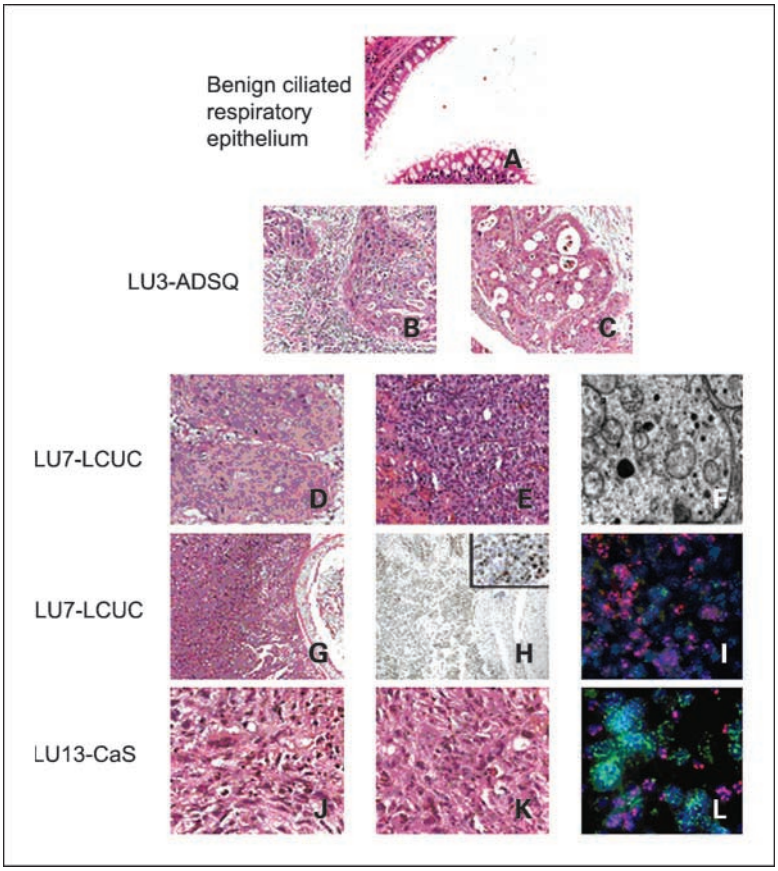

Fig. 2. Representative H&E stained tissues of: *A,* grafted benign ciliated respiratory epithelium (*LU1,2*); *B* and *C,* pregrafted and postgrafted tumor tissues, respectively, from a case of adenosquamous carcinoma (*LU3-ADSQ*); *D,* pregraft tissue from a mixed squamous cell and large-cell undifferentiated carcinoma and corresponding xenograft; *E,* LU7-LCUC, showing large cell morphology with local tissue invasion; *F,* transmission electron photomicrograph of cell cytoplasm of LU7-LCUC showing occasional neuroendocrine granules (courtesy of Dr. E. Cutz); *G,* representative H&E stained mouse lung tissue from a host grafted with LU7-LCUC, showing an enlarged peribronchial lymph node; *H,* containing metastatic human cells as shown by immunoreactivity for human-specific antimitochondrial antibody and Ki-67 antibody (*inset*); *I,* demonstration of human metastatic cells in the liver of a host mouse grafted with LU7-LCUC by use of species-specific pan-centromeric FISH probes; mouse cell nuclei are detected with Cy3-labeled mouse probes (*pink*) whereas human tumor cell nuclei are detected by FITC-labeled human probes (*green*); *J* and *K,* representative H&E stained tissues of pregrafted and postgrafted tumor tissues, respectively, from lung carcinosarcoma (*LU13-CaS*); *L,* FISH labeling showing the presence of numerous mouse stromal infiltrating cells (*pink*) among human tumor cells (*green*) in a graft of LU13-CaS.

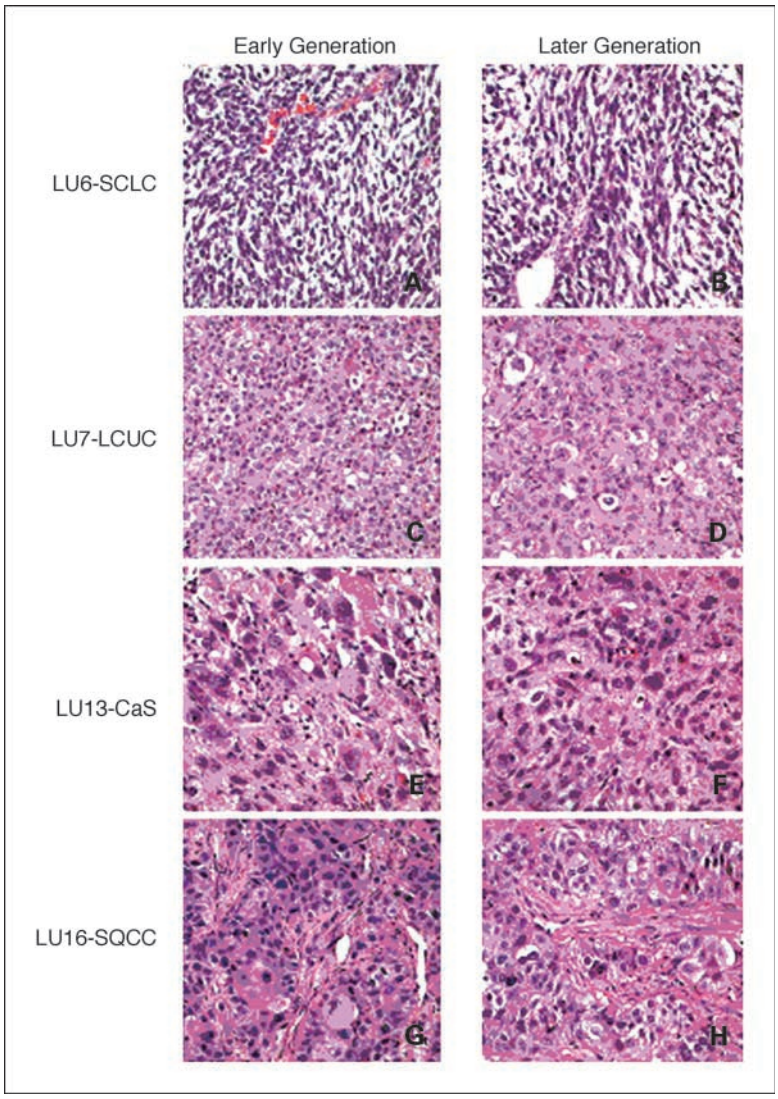

Fig. 3. Representative H&E stained tissue of the four transplantable lung tumor lines: early (second) generation tumor tissue grafts (*left*) and corresponding later-generation (fifth or later) xenografts (*right*) for cases of small cell carcinoma (*LU6-SCLC*; *A* and *B*), large cell undifferentiated carcinoma (*LU7-LCUC*; *C* and *D*), sarcoma (*LU13-CaS*; *E* and *F*), and poorly differentiated SQCC (*LU16-SQCC*; *G* and *H*). Original magnification, ×40.

maintenance of the 2n ploidy status in the early and late xenografts. For LU13-CaS, pregraft tumor tissue was only available for CGH and FISH (Table 3). CGH showed several genomic changes corresponding to the karyotypic complexity seen by SKY analysis in the early xenograft. Interphase FISH of the original tumor revealed a range of ploidy, between 3n and 4n. For centromere 3, a majority of the cells showed more than four signals, corresponding to the gain of chromosome 3 detected by CGH (Table 3). Similarly, the original tumor specimen corresponding to LU16-SQCC showed a ploidy status (3n) consistent with the SKY results of the xenograft (Table 3). In most cases, three or four hybridization signals could be detected for each of the centromere probes, in keeping with the detected range of ploidy by SKY (Fig. 5H). In the case of the locus-specific probe for 9p21, the original tumor typically displayed two hybridization signals against a predominantly triploid background (Fig. 5H, inset). The SKY findings of the early graft showed a clonal loss of 9p in one of the three chromosome 3 homologues (Fig. 5A), strengthening proof for the faithful representation of the original tumor in the early xenografts.

Discussion

Models based on SRC xenografts of human tumor tissue offer several advantages. One of the most important benefits is the preservation of tumor tissue histology, both relative to the original clinical sample, and over successive xenograft generations. In the SRC xenografts, the original tumor stroma is included and later expanded by equivalent host stromal elements, as shown in this study by the appearance of murine stroma in transplantable human tumor lines. Tumor stroma seems to be essential for well-differentiated or low-grade neoplasms that depend on complex stromal-epithelial relationships for growth (18) and it seems likely that the inclusion of stroma in the SRC xenografts is important in preserving the tumor tissue architecture. With the current SRC model, it is possible to establish relatively early stage or well-differentiated neoplasms *in vivo* with the potential to study their progression under defined experimental conditions.

Another significant advantage of SRC tissue xenografting is that it can provide a continuous source of live, transplantable tumor tissue generated from minute amounts of biopsy

Table 3. Summary of molecular cytogenetic findings in four transplantable xenograft lines

	SKY	CGH	FISH
LU6-SCLC			
Early graft	36-40, X, −Y, del(3)(p12), +del(3)(p?)(q?), i(5)(q11), der(7)(7;19 or 20)(q31;?), der(8)(8pter→8qter→8q24→8qter), der(8)(21pter→qter::8pter→qter→8q24→qter), der(9)t(8;9)(q11;p11), dup(10)(q?), der(11)(20?→20?::11?→11?::20?→20?::11p11→q?::20?→20?::11?→11?), i(14)(q11), der(17)t(17;18)(p11;q?), −18, −19, −19, −20, −20[cp5]	+5q14-q23, −8p, amp8q13, amp8q23, −9p, +11p11-p12, +12q13-q14	Paraffin FISH confirms high-level MYCC (8q24) amplification
Late graft	40 with the retention of del(3)(p12), +del(3)(p?)(q?), i(5)(q11), der(7)(7;19 or 20)(q31;?), der(8)(8pter→8qter→8q24→8qter), der(8)(21pter→qter::8pter→qter→8q24→qter), der(9)t(8;9)(q11; p11), der(11)(20?→20?::11?→11?::20?→20?::11p11→q?::20?→20?::11?→11?), i(14)(q11), der(17)t(17;18)(p11;q?) [cp3]	−8p, amp8q13, amp8q23, amp12q, +13, −17p, −18q, −X	Paraffin FISH confirms high-level MYCC (8q24) amplification
LU7-LCUC			
Tumor before graft	No material available	−1p36-pter +4p, +5, +8q, +10, +12p, −12q24-qter, +13, −X	Paraffin FISH using cen 3, cen7, cen17 and p19 (9p21) confirms diploid status of tumor, with all cells showing two copies per cell
Early graft	45-46, XY, +der(1)t(1;13)(p11;q11), +der(1)t(1;18)(q11;p11), der(6)t(2;6)(?;p23), +13, der(17)t(8;17)(q?;p12), −17, −18[cp4]	−1p36-pter, +5, +8q, −12q24-qter, +13, −X	Paraffin FISH confirms low-level gain of MYCC (8q24)
LU13-CaS			
Tumor before graft	No material available	−1p35-pter, +1q31-qter, +2p, −2q34-2qter, +3, +4q11-q28, −4q32-q35, amp5p, −5q33-qter, −6q21-qter, −8p, +8q, +9p, −9q, −11q22-qter, amp12p, +13, −16p, +17q11-q23	Paraffin FISH using cen 3, cen7, cen17 and p19 (9p21) confirms 4n+/− status of tumor consistent with CGH and SKY findings
Early graft	Incomplete due to karyotypic complexity 76-98 ‹4n›dic(Y;11)(p11.3;q25), +1, +1, + der(2)t(2;22) (p11;q11), +3, +3, +der(4)t(4;18)(qter;?), dic(5;7)(q35:p22) +der(8)(8pter→8q11::4q?→4q?::8q11→8q22→8q11→8q22→8qter::?4q?→?4q?), +dup(8)(q21q24), der(12)t(12;15)(p11;q11), der(15)t(3;15)(p11;p11), +der(20)(8?→8?::3?→3?::20p11→20qter), +der(20)t(3 or 6;20)(?:p11), der(22)t(3;22)(?;p11)*	Poor DNA quality	Paraffin FISH confirms low-level gain of MYCC (8q24)
LU16-SQCC			
Tumor before graft	No material available	Poor DNA quality	Paraffin FISH using cen 3, cen7, cen17 and p19 (9p21) confirms 3n+/− status of tumor consistent with SKY findings

(*Continued on the following page*)

Table 3. Summary of molecular cytogenetic findings in four transplantable xenograft lines (Cont'd)

	SKY	CGH	FISH
Early graft	56-67‹3n›, −X, −X,Y, del(1)(p12), del(1)(p?)(q?), der(2)dic(2;5) (q37;q11.2), −2, +der(3)t(1;3)(?;p?), +i(3)(q10), +del(3)(p?), del(4) (p?)(q?), −4, dup(5)(q?), der(5)t(5;11?)(q35:q?), −5, der(6)(7?→7?:: 13q?→13q?::6p22→qter), der(6)(6pter→6qter::13q11→13qter), del(7)(p?)(q?), dup(7)(q11q36), −7, der(8)(7?→7?::13q?›13q::8p22?→8qter), del(8)(p?)(q?), der(8)(7?→7?::8q21→8q24), del(9)(p21), ins(10;5)(q21;?), −10, der(12)t(5;12)(p?;p13), der(13) t(8;13)(q21;q14), der(13)t(8;130)(q31;?), +der(13)(8pter→p11::13p11→13q14::7p15?→pter), der(15)t(9;15)(?;p11), del(15)(q?), +der(15)t(13;or18)(?;p11), del(16)(p?)(q?), del(16)(p?0, der(17)t(13or18);17)(?;p?)X2, del(18)(p?)(q?), der(19)t(11;19)(q11;p11), +der(20)t(?;20)(?;p11), −21, −21, der(21)t(X;21)(q11;p11)X2 [cp5]	Poor DNA quality	Paraffin FISH confirms low-level gain of MYCC (8q24)

NOTE: The SKY results are expressed as a composite karyotype according to the guidelines of the 1995 International Standards for Human Cytogenetic Nomenclature (15).

*Many nonclonal complex aberrations were identified, often involving two or more chromosomal partners. Also, almost all chromosomes were represented as small nonclonal and likely clonal chromosomal fragments. Nonclonal ring, dicentric chromosomes, and bi-, tri-, and quadraradial formations were detected. Some 8n cells were also present.

material and surgical specimens. Using this method, we achieved a very high engraftment rate (>95%) of primary human lung tumors and benign tissue, providing a potential source of live tissue for use in a variety of applications. The success of the SRC model can be contrasted with the approach of directly growing xenografts orthotopically, which is typically associated with higher failure rates and host mortality as a result of the invasive thoracotomy procedure required for xenografting (19). Such an approach would incur a high risk of losing precious scanty biopsy material due to graft failure or postoperative complications. An alternative approach when an orthotopic model is desired would be to first generate ample xenograft tissue via the SRC method followed by orthotopic grafting. For example, this approach would be particularly useful when studying mechanisms of tumor metastasis and tumor-stromal interactions within the lung. In the present study, the relative lack of metastatic activity observed in mice carrying SRC xenografts from patients with metastatic disease may be due to the limited time of the assays used (2 months). It is possible that tumor subclones with the ability to metastasize require additional time to emerge. In addition, the nature of the microenvironment of the SRC graft site may differ sufficiently from that of the lung such that metastatic clones do not readily develop. Additional studies using longer observation periods of SRC xenografts as well as combined SRC-orthotopic models would be needed to address these hypotheses. It is interesting to note, however, that in a study also conducted by our group, orthotopic grafts of prostate cancer, generated first by the SRC method, do produce metastatic tumors (11).

One drawback of any tumor grafting model, however, is that small samples may not always be representative of an entire tumor. In a few cases, the xenografts obtained did not yield the expected tissue type, as found for one graft of a carcinoid tumor (LU9) and one of a SCLC (LU12), in which only fibrous stroma was found 2 months postgrafting. In another case, the large cell morphology of LU7-LCUC only reflected part of the histologic spectrum exhibited by the original tumor, which also featured a significant component of squamous differentiation. In the case of the carcinosarcoma, a sarcoma tumor line developed without an epithelial component. These apparently discrepant results seem to reflect nonrepresentative sampling of the original surgical specimens or tissue fragments, which were minute in the case of biopsy material. Where possible, use of multiple samples from the same tumor could circumvent this problem. Nonetheless, in the vast majority of cases in this study, the xenografts seemed representative of the original tissues, with their growth rates reflecting the aggressiveness or indolence of the tumor in the patient.

Another advantage of using SRC tissue xenografts lies in their ability to recapitulate the general phenotypic and genotypic characteristics of the tumors from which they originate. In the present retrospective and partially prospective study, we examined the fidelity of SRC lung cancer xenograft models and their potential usefulness for monitoring genomic changes under various experimental conditions. Histologic analysis showed that both slow- and fast-growing primary lung cancer tissue xenografts during the first 2 months of grafting were very similar to the original tumors and were stable over successive graft generations. As such, they show a similar behavior to SRC xenografts of human prostate and ovarian cancers previously described (7, 10). Using transplantable tumor lines developed from fast-growing lung cancer xenografts, it was possible to monitor changes in chromosomal structure and CGH profiles of the tumor cells over time and successive graft generations. Follow-up studies giving attention to additional variables, such

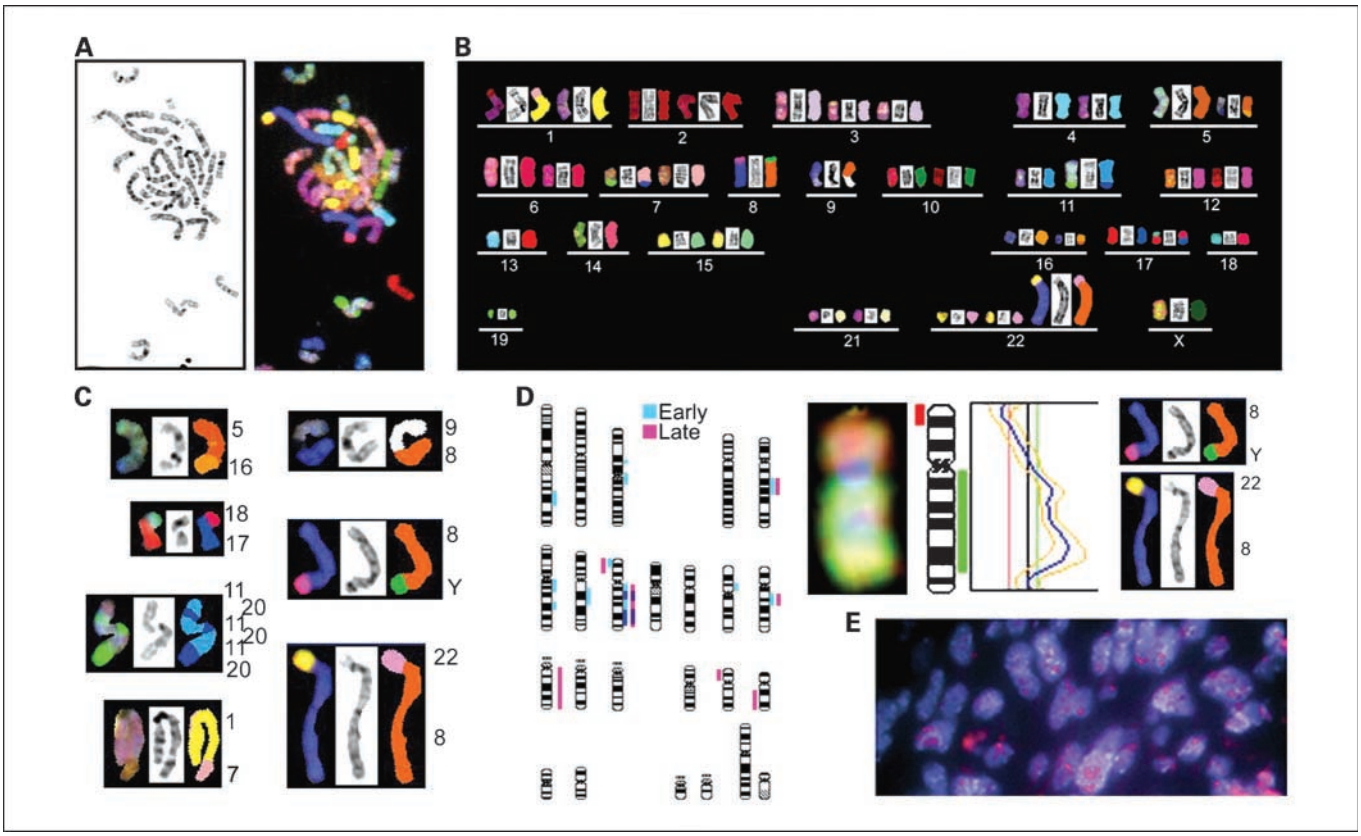

Fig. 4. Molecular cytogenetic analysis for LU6-SCLC. *A,* hybridization of a metaphase spread with the SKY painting probes. Left, inverted DAPI; right, hybridized metaphase spread. *B,* karyotype showing the RGB (red-green-blue) chromosome, inverted DAPI chromosome, and classified (pseudocolored) chromosome. *C,* highlights of translocations as revealed by SKY. *D,* summary of CGH findings from the early xenograft and late xenograft and correlation of amplified regions of 8q to SKY results. *E,* interphase FISH using MYCC of the early xenograft confirming amplification of MYCC.

as gene expression, will provide additional information on the biological behavior of the tumor lines.

The specific molecular cytogenetic data obtained in this study add to the limited data reported to date for lung cancer using SKY or multicolor FISH (20–28). The most common cytogenetic aberrations described in SCLC [reviewed by Balsara and Testa (29)], include complete or regional loss of 3p, loss of 5q, or numerical loss of chromosome 5. Loss of 13q and 17p are also frequent. The karyotypic changes are usually quite extensive, and the modal chromosome numbers are typically in the triploid range. The pattern of chromosomal complexity and genomic changes seen in small cell lung cancers was also identified in LU6-SCLC. SKY and CGH of the early and late generation xenograft showed that the ploidy and structural changes were maintained. However, the later xenograft generation CGH profile was found to show some changes not identified in the early xenograft, including gain of chromosome 13 and loss of 17p, 18q, and X. In addition, the gain of 5q14-q23 detected in the early xenograft was not identified in the later xenograft. These findings suggest that the transplanted tumors are undergoing genomic change over time and with successive transplantation. Although the tumor genome exhibited copy number changes, the detected changes were, in general, consistent with the genomic changes known about this tumor subtype. This finding begs the question as to whether the original tumor, if left to progress in its human host, would have proceeded to display the same cytogenetic profiles detected in the xenograft model. In addition to the common changes, amplification of 8q and high-level amplification of the regions 8q13 and 8q23/24 were identified. Subsequent FISH analysis confirmed the amplification of MYCC in a pattern consistent with homogeneously staining regions (Fig. 4E). The formation of double minutes or homogeneously staining regions leading to gene amplification (of MYC family genes) has been seen most frequently in SCLC cell lines and tumors from treated rather than untreated patients (29, 30), such as LU6-SCLC, which was derived from a patient who had received two different treatment courses prior to tumor xenografting. The amplification of MYCC in the early graft and later generation graft suggests that MYCC amplification may influence the high proliferation rate detected in this tumor (31).

As reviewed by Balsara and Testa (29), molecular cytogenetic analysis of NSCLC xenografts has revealed complex chromosomal aberrations with multiple numerical and structural changes, with karyotypes that are often near-triploid. Structural rearrangements have been shown to be complex and the result of unbalanced translocations. Prominent numerical changes include losses of chromosomes 9 and 13, as well as loss of chromosome Y in males. Gain of chromosome 7 is also a frequent numerical change and has been proposed to be a very early change in NSCLC, and may be found in premalignant lung tissue in a subset of patients (29). Of the NSCLCs examined in the present study, the locally aggressive and

metastatic tumor, LU7-LCUC, surprisingly showed a relatively less complicated pattern of chromosomal aberrations. The CGH profile of the original tumor was found to be consistent with the pattern of genomic changes observed in the early xenograft. In addition, interphase FISH using several centromere probes confirmed the maintenance of the ploidy status of the tumors in the early xenografts. In the case of the carcinosarcoma tumor, the early graft, LU13-CaS, showed complex structural changes, often involving three or more chromosomes, in addition to the presence of dicentric and ring chromosomes as well as the presence of triradial chromosomes (Fig. 5C, inset). The overall ploidy of this tumor line was found to be near-tetraploid, although some spreads were characteristic of near-octaploidy, suggesting the failure of cytokinesis. This is consistent with the histologic finding of aberrant mitotic figures, multilobed nuclei, and multinucleation. Interphase

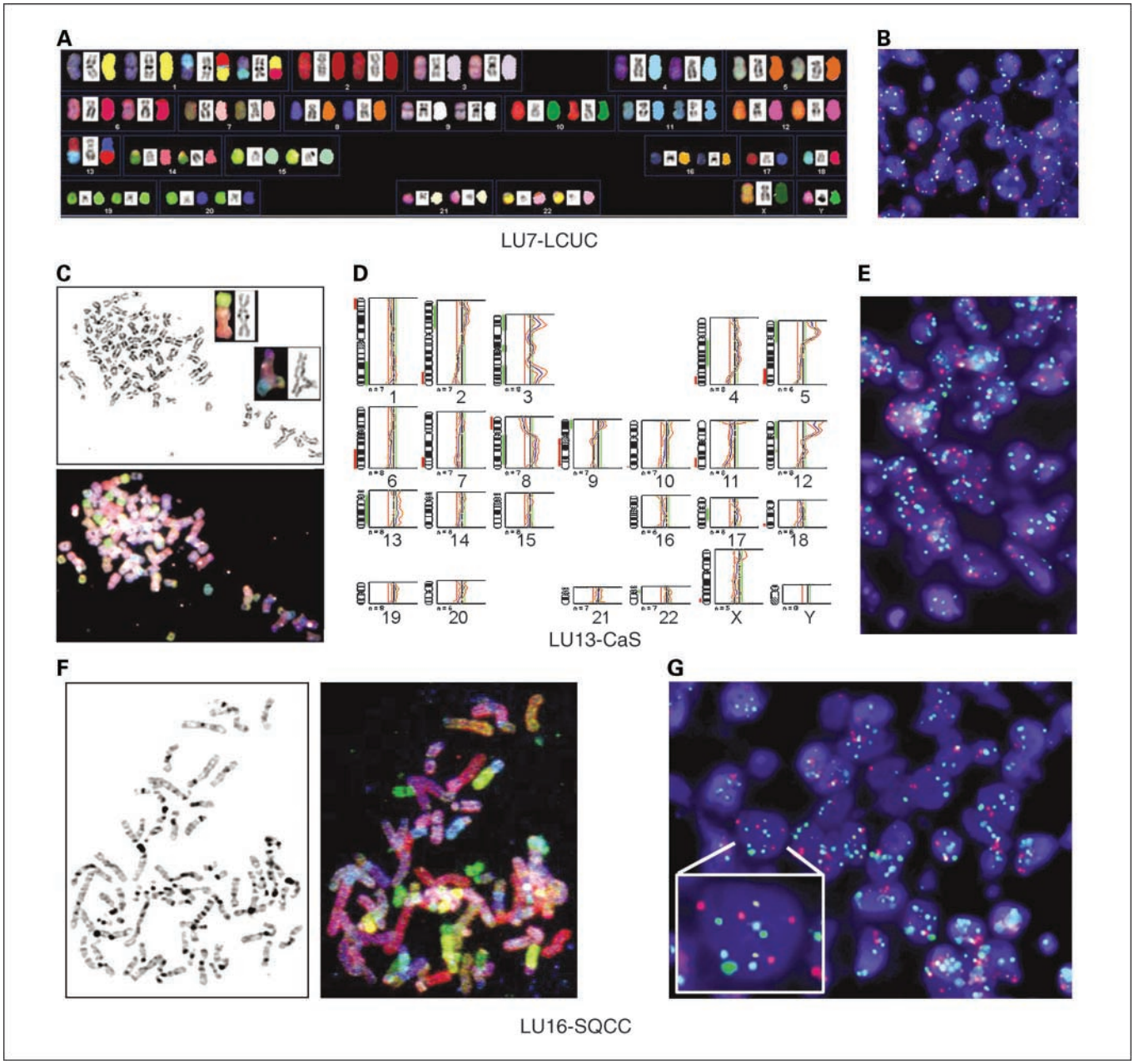

Fig. 5. Molecular cytogenetic findings from LU7-LCUC, LU13-CaS, and LU16-SQCC. LU7-LCUC: *A,* SKY karyotype showing RGB, inverted DAPI, and classified chromosomes. *B,* interphase FISH using centromeres 3 (*red*), 7 (*green*), 17 (*light blue*), and 9p21 (*yellow*) of the original patient tumor confirming the diploid nature of the original specimen compared with the early xenograft. LU13-CaS: *C,* representative inverted DAPI (*top*) and SKY-hybridized (*bottom*) metaphase spread. Inset, complex structural aberrations including a dicentric chromosome and triradial chromosome. *D,* CGH results of the original patient tumor showing copy number changes consistent with SKY findings (Table 3). *E,* interphase FISH using centromeres 3 (*red*), 7 (*green*), 17 (*light blue*), and 9p21 (*yellow*) of the original patient tumor confirming the triploid/tetraploid nature of the original specimen compared with the early xenograft. LU16-SQCC: *F,* representative inverted DAPI (*left*) and SKY-hybridized (*right*) metaphase spread. *G,* interphase FISH using centromeres 3 (*red*), 7 (*green*), 17 (*light blue*), and 9p21 (*yellow*) of the original patient tumor confirming the triploid/tetraploid nature of the original specimen compared with the early xenograft. Inset, magnified nucleus showing four red signals (centromere 3), three green signals (centromere 7), three light blue signals (centromere 17), and two yellow signals (9p21) consistent with SKY findings.

FISH of the original tumor showed that its ploidy status was the same as that of the engraftments and confirmed CGH findings. Finally, the squamous cell carcinoma, LU16-SQCC, also showed a complex karyotype consistent with findings from other cytogenetic descriptions of SQCCs (23). FISH analysis of the original tumor specimen was consistent with the SKY findings in the xenograft, specifically, the detection of two copies of 9p21 in the original specimen corresponding to the clonal loss of 9p in one of the three chromosome 9 homologues. The net loss of 9p21 in this tumor is consistent with the finding of 9p deletions in NSCLCs with the loss of 9p proposed as a critical change in this neoplasm, and a critical chromosomal alteration that distinguishes SCLCs from NSCLCs (29).

As indicated by this study, SRC xenograft methodology can readily lead to the expansion of cancer subpopulations. As such, it could be particularly useful for studies on cancer stem cells, thought to be the primary cause of disease recurrence, therapy resistance, and distant metastasis [reviewed by Bonnet (32) and Soltysova et al. (33)]. Few cancer stem cell studies have been conducted in lung cancer (34, 35). However, Kim et al. (35) have recently shown the existence of a regional pulmonary stem cell population, termed bronchioalveolar stem cells. Because cancer stem cell populations typically constitute <1% of tumor cells, isolation of these cells from primary tumors is extremely difficult. The SRC xenograft system can potentially provide a useful means for the expansion, identification, and analysis of representative lung cancer stem cells.

The present study indicates that SRC grafting of lung tumor tissues is a versatile method for generating sufficient representative tissues for enhanced comprehensive genomic and proteomic analysis of lung cancers, particularly with respect to tumor progression and treatment resistance. Application of this model may ultimately enable investigators to develop more successful targeted treatment strategies.

Acknowledgments

The authors thank Yuwei Wang and Rebecca Wu (BC Cancer Research Centre) for excellent technical assistance, Dr. Annette McWilliams (BC Cancer Centre, Vancouver, Canada) for help in clinical data collection, Paula Marrano (Squire Lab, Princess Margaret Hospital/University Health Network, Toronto, Ontario, Canada) for her assistance in the interpretation of SKY data, Dr. Ernest Cutz (Department of Pathology, Hospital for Sick Children, Toronto, Canada) for electron microscopy, and Dr. Ming-Sound Tsao (Department of Pathology, University Health Network/Princess Margaret Hospital, Toronto, Canada) for helpful suggestions.

References

1. Travis WD. Pathology of lung cancer. Clin Chest Med 2002;23:65–81.
2. Kerbel RS. Human tumor xenografts as predictive preclinical models for anticancer drug activity in humans: better than commonly perceived—but they can be improved. Cancer Biol Ther 2003;2:S134–9.
3. Gazdar AF, Oie HK. Cell culture methods for human lung cancer. Cancer Genet Cytogenet 1986;19:5–10.
4. Phelps RM, Johnson BE, Ihde DC, et al. NCI-Navy Medical Oncology Branch cell line data base. J Cell Biochem Suppl 1996;24:32–91.
5. Bhowmick NA, Neilson EG, Moses HL. Stromal fibroblasts in cancer initiation and progression. Nature 2004;432:332–7.
6. Voskoglou-Nomikos T, Pater JL, Seymour L. Clinical predictive value of the *in vitro* cell line, human xenograft, and mouse allograft preclinical cancer models. Clin Cancer Res 2003;9:4227–39.
7. Wang YZ, Revelo MP, Sudilovsky D, et al. Development and characterization of efficient xenograft models for benign and malignant human prostate tissue. Prostate 2005;64:149–59.
8. Bogden AE, Haskell PM, LePage DJ, Kelton DE, Cobb WR, Esber HJ. Growth of human tumor xenografts implanted under the renal capsule of normal immunocompetent mice. Exp Cell Biol 1979;47:281–93.
9. Liou LS, Zhou Y, Wang Y, et al. A living human tumor bank using an orthotopic xenograft mouse model: feasibility and implications of angiogenesis and proliferation [abstract]. J Urol 2004;171:208.
10. Lee CH, Xue H, Sutcliffe M, et al. Establishment of subrenal capsule xenografts of primary human ovarian tumors in SCID mice: potential models. Gynecol Oncol 2005;96:48–55.
11. Wang Y, Xue H, Cutz J-C, et al. An orthotopic metastatic prostate cancer model in SCID mice via grafting of a transplantable human prostate tumor line. Lab Invest 2005;85:1392–404.
12. Bayani J, Squire JA. Cell Biology of Chromosomes and Nuclei. In: Morgan K, editor. Current Protocols in Cell Biology. New York (NY): John Wiley and Sons Inc.; 2004. p 22.2.1–11.
13. Bayani J, Zielenska M, Pandita A, et al. Spectral karyotyping identifies recurrent complex rearrangements of chromosomes 8, 17, and 20 in osteosarcomas. Genes Chromosomes Cancer 2003;36:7–16.
14. Schrock E, du Manoir S, Veldman T, et al. Multicolor spectral karyotyping of human chromosomes. Science 1996;273:494–7.
15. Mitelman F. ISCN 1995 An international system for human cytogenetic nomenclature (1995). New York: S. Karger; 1995.
16. Klein CA, Schmidt-Kittler O, Schardt JA, Pantel K, Speicher MR, Riethmuller G. Comparative genomic hybridization, loss of heterozygosity, and DNA sequence analysis of single cells. Proc Natl Acad Sci USA 1999;96:4494–9.
17. Stoecklein NH, Erbersdobler A, Schmidt-Kittler O, et al. SCOMP is superior to degenerated oligonucleotide primed-polymerase chain reaction for global amplification of minute amounts of DNA from microdissected archival tissue samples. Am J Pathol 2002;161:43–51.
18. Van Kempen LC, Ruiter DJ, van Muijen GN, Coussens LM. The tumor microenvironment: a critical determinant of neoplastic evolution. Eur J Cell Biol 2003;82:539–48.
19. Hoffman RM. Orthotopic metastatic mouse models for anticancer drug discovery and evaluation: a bridge to the clinic. Invest New Drugs 1999;17:343–59.
20. Sy SM, Wong N, Lee TW, et al. Distinct patterns of genetic alterations in adenocarcinoma and squamous cell carcinoma of the lung. Eur J Cancer 2004;40:1082–94.
21. Luk C, Tsao MS, Bayani J, Shepherd F, Squire JA. Molecular cytogenetic analysis of non-small cell lung carcinoma by spectral karyotyping and comparative genomic hybridization. Cancer Genet Cytogenet 2001;125:87–99.
22. Berrieman HK, Ashman JN, Cowen ME, Greenman J, Lind MJ, Cawkell L. Chromosomal analysis of non-small-cell lung cancer by multicolour fluorescent *in situ* hybridisation. Br J Cancer 2004;90:900–5.
23. Ashman JN, Brigham J, Cowen ME, et al. Chromosomal alterations in small cell lung cancer revealed by multicolour fluorescence *in situ* hybridization. Int J Cancer 2002;102:230–6.
24. Grigorova M, Lyman RC, Caldas C, Edwards PA. Chromosome abnormalities in 10 lung cancer cell lines of the NCI-H series analyzed with spectral karyotyping. Cancer Genet Cytogenet 2005;162:1–9.
25. Tai AL, Fang Y, Sham JS, et al. Establishment and characterization of a human non-small cell lung cancer cell line. Oncol Rep 2005;13:1029–32.
26. Sy SM, Fan B, Lee TW, et al. Spectral karyotyping indicates complex rearrangements in lung adenocarcinoma of nonsmokers. Cancer Genet Cytogenet 2004;153:57–9.
27. Dennis TR, Stock AD. A molecular cytogenetic study of chromosome 3 rearrangements in small cell lung cancer: consistent involvement of chromosome band 3q13.2. Cancer Genet Cytogenet 1999;113:134–40.
28. Sargent LM, Senft JR, Lowry DT, et al. Specific chromosomal aberrations in mouse lung adenocarcinoma cell lines detected by spectral karyotyping: a comparison with human lung adenocarcinoma. Cancer Res 2002;62:1152–7.
29. Balsara BR, Testa JR. Chromosomal imbalances in human lung cancer. Oncogene 2002;21:6877–83.
30. Brennan J, O'Connor T, Makuch RW, et al. Myc family DNA amplification in 107 tumors and tumor cell lines from patients with small cell lung cancer treated with different combination chemotherapy regimens. Cancer Res 1991;51:1708–12.
31. Zajac-Kaye M. Myc oncogene: a key component in cell cycle regulation and its implication for lung cancer. Lung Cancer 2001;34:S43–6.
32. Bonnet D. Cancer stem cells: lessons from leukaemia. Cell Prolif 2005;38:357–61.
33. Soltysova A, Altanerova V, Altaner C. Cancer stem cells. Neoplasma 2005;52:435–40.
34. Otto WR. Lung epithelial stem cells. J Pathol 2002;197:527–35.
35. Kim CF, Jackson EL, Woolfenden AE, et al. Identification of bronchioalveolar stem cells in normal lung and lung cancer. Cell 2005;121:823–35.